GaN HBT: Toward an RF Device

Lee S. McCarthy, Ioulia P. Smorchkova, Huili Xing, P. Kozodoy, Paul Fini, J. Limb, David L. Pulfrey, *Fellow, IEEE*, James S. Speck, Mark J. W. Rodwell, *Senior Member, IEEE*, S. P. DenBaars, *Member, IEEE*, and U. K. Mishra, *Fellow, IEEE*

***Abstract*—This paper reviews efforts to develop growth and fabrication technology for the GaN HBT. Conventional devices are grown by plasma assisted MBE on MOCVD GaN templates on sapphire. HBTs were fabricated on LEO material identifying threading dislocations as the primary source of collector-emitter leakage which was reduced by four orders of magnitude for devices on nondislocated material. Base doping studies show that the mechanism of this leakage is localized punch-through caused by compensation near the dislocation. High contact and lateral resistance in the base cause large parasitic common emitter offset voltages (from 1 to 5 V) in GaN HBTs. The effect of this voltage drop in common emitter characteristics is discussed. The combination of this voltage drop and the emitter collector leakage make Gummel and common base characteristics unreliable without verification with common emitter characteristics. The selectively regrown emitter bipolar transistor is presented with a dc current gain of 6 and early voltage greater than 400 V. The transistor operated to voltages over 70 V. This device design reduces base contact resistance, and circumvented difficulties associated with the emitter mesa etch process. The Mg memory effect in MOCVD grown GaN HBTs is discussed, and MBE grown device layers are shown to produce sharp doping profiles. The low current gain of these devices, (3–6) is discussed, and an HBT with a compositionally graded base is presented, as well as simulations predicting further current gain improvements with base grading.**

***Index Terms*—Base grading, bipolar, common base, common emitter, compensation, current gain, GaN, Gummel, HBT, leakage, LEO, MBE, memory effect, Mg, MOCVD, offset, regrowth, RIE, threading dislocations, transistor.**

Manuscript received April 1, 2000; revised November 3, 2000. This work was supported by a grant from the U.S. Office of Naval Research. The review of this paper was arranged by Editor U. K. Mishra.

L. S. McCarthy was with the Electrical and Computer Engineering Department, University of California, Santa Barbara, CA 93106 USA. He is now with Nitronex Corporation, Raleigh, NC 27606 USA (e-mail: lee_mccarthy@nitronex.com).

I. P. Smorchkova, H. Xing, M. J. W. Rodwell, and U. K. Mishra are with the Electrical and Computer Engineering Department, University of California, Santa Barbara, CA 93106 USA.

P. Fini, and J. Speck are with the Materials Department, University of California, Santa Barbara, CA 93106 USA.

P. Kozodoy was with the Electrical and Computer Engineering Department, University of California, Santa Barbara. He is now with Cree Lighting, Goleta, CA 93117 USA.

J. Limb was with the Electrical and Computer Engineering Department, University of California, Santa Barbara, CA 93106 USA. He is now with the Korean Military Academy, South Korea.

D. Pulfrey was with the Electrical and Computer Engineering Department, University of California, Santa Barbara, CA 93106 USA. He is now with the Department of Electrical Engineering, University of British Columbia, Vancouver, BC V6T 1Z4 Canada.

Publisher Item Identifier S 0018-9383(01)01466-6.

I. INTRODUCTION

THE PAST several years have seen a dramatic increase in research of GaN materials and devices. Progress has been made in areas including rf electronic devices such as FETs[1] and bipolar transistors [2]–[5] as well as optoelectronics devices including light emitters, lasers [6] and detectors [7]. GaN is desirable for electronics applications due to saturated electron velocities of 2×10^7 cm/s [8], and its 3.4 eV bandgap which leads to a critical breakdown field of 2 MV/cm [9], and stability at high temperatures. As demonstrated in other III–V material systems, HBTs offer several important advantages over FETs. HBTs generally have better threshold uniformity and device linearity, as well as lower phase noise than FETs. In addition, the HBT structure inherently offers a higher ratio of output current to parasitic capacitance.

There have been several reports of GaN HBTs in the literature [2]–[5], but the results are still preliminary. The fundamental material properties described in Table I can be used in comparison with a mature material system to predict potential rf performance of these devices. Lee *et al* demonstrated AlInAs/GaInAs HBTs using a transferred substrate Schottky collector technology with a power gain cut-off frequency, $f_{\max}$, of 820 GHz [10]. If this technology were applied to a GaN bipolar structure with a 50 nm base, having a base carrier concentration of 5×10^{19} cm^{-3}, and a 100 nm thick collector, the predicted $f_{\max}$ is 200 GHz with a current gain cutoff frequency, f_t, of 200 GHz, and a 15 V breakdown voltage. For power switching applications, material properties suggest that a 1 kV device with a collector thickness of 7 μm, and a base thickness of 200 nm would have an f_t of 6 GHz and an $f_{\max}$ over 300 GHz. This paper presents many of the relevant issues to the development of the GaN bipolar transistor. We discuss the progress and current status of GaN bipolar growth and processing technologies, and suggest future directions for the realization of rf device performance in the HBT.

II. DEVICE DETAILS

A typical device structure used in these experiments along with a simulated band diagram is shown in Fig. 1. Device structures were grown by plasma assisted MBE on MOCVD GaN templates on sapphire. The use of MBE versus MOCVD growth for the active layers is discussed in Section VIII. The emitter was $Al_{0.1}Ga_{0.9}N:Si$ ($N_D = 10^{18}$ cm^{-3}) with a GaN : Si emitter contact layer. The base layer was 100 nm GaN : Mg, $N_A = 5 \times 10^{19}$ cm^{-3}. Magnesium is a deep accepter, $E_A - E_V \approx$ 110–200 meV [11], resulting in a carrier concentration of $p = 8 \times 10^{17}$ cm^{-3} for this accepter density. The collector was 500 nm unintentionally doped (UID) GaN

0018–9383/01$10.00 © 2001 IEEE

TABLE I
COMPARISON OF MATERIAL PROPERTIES RELEVANT TO RF PERFORMANCE

Property	*GaN*	*GaInP*	*Si*
v_{sat} [cm/s]	20×10^6	10×10^6	6×10^6
E_{crit} [MV/cm]	2	0.6	0.3

with a background donor concentration of 5×10^{16} cm^{-3}. The subcollector is GaN : Si, $N_D = 10^{18}$ cm^{-3}. Emitter and collector contacts are Ti/Al/Ni/Au, while the base contacts are Pd/Au. For conventional devices, the mesas were etched with a chlorine reactive ion etch (RIE).

Although there are reports of higher hole concentrations using co-doping of Mg with oxygen or silicon [12], electronic device results with this doping technology have not been reported. Holes in GaN, with an effective mass of $2.2 \cdot m_0$ [13], have mobilities between 5 and 20 cm^2/Vs in highly doped GaN : Mg layers. Consequently, the base of an NPN transistor has a resistivity on the order of 1 Ω cm, with a sheet resistivity for a 100 nm base of 100 kΩ/□. This low base conductivity increases the parasitic base resistance, R_{BB}, degrading rf performance and contributing to the current-crowding effect in the base-emitter junction. In addition, the p-GaN surface is sensitive to etch damage. The Cl_2 RIE used to access the base layer is primarily physical, and is believed to cause point defects, creating states donors, degrading contacts to etched p-type GaN. Although contact resistances as low as 2×10^{-5} Ω· cm^{-2} [14] have been reported on p-type GaN, contacts to Cl_2-RIE etched p-GaN shown in Fig. 2 have a voltage barrier of 10 V.

The regrown base HBT reduces the contact voltage barrier to the p-GaN surface (Fig. 2). After the RIE emitter mesa etch, the emitter was capped with a dielectric mask, AlN_x. In addition to protecting the emitter mesa during the MOCVD growth, the AlN_x mask is selective to GaN growth, and chemically inert in the reducing $NH_3 + H_2$ environment. The etch damage is buried with the new GaN : Mg growth, resulting in an improvement in contact quality as well as increased base conductivity. Used in conjunction with a low-etch-damage RIE process, the base contact voltage barrier is as low as 1 V (Fig. 2). A further improvement in base-contact quality is attainable with the regrown emitter HBT (Section IV).

III. OFFSET VOLTAGE

The effect of the poor base conductivity and contact voltage barrier is apparent in the common emitter offset voltage. The offset voltage is the collector-emitter voltage in the common emitter mode where the net collector current becomes positive. At this point, both the base-emitter and base-collector diodes are forward biased. The collector current saturates as the base-collector diode becomes reverse biased. The parasitic offset voltage observed in the GaN HBT is explained as follows:

Because of a high voltage drop across the base contact and a high lateral resistance, the voltage of the base layer under the contact is substantially higher than the voltage of the base in the active device Fig. 3). This effectively divides the area under the emitter and the area under the base contact into two devices—the active transistor and a parasitic base-collector diode.

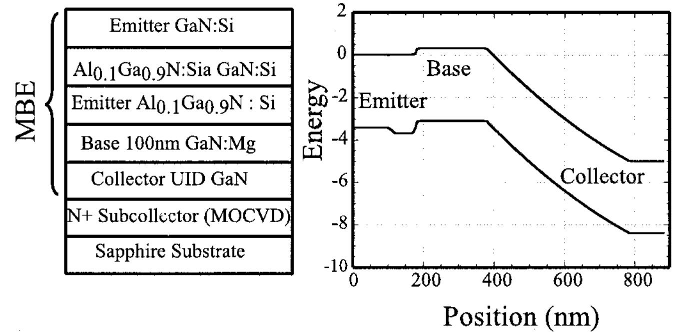

Fig. 1. Left: Typical structure for AlGaN/GaN HBT grown by plasma assisted MBE on MOCVD GaN on sapphire. The collector is unintentionally doped (UID) GaN $N_D \approx 5 \times 10^{16}$ cm^{-3}. Right: Simulated band diagram of typical device. The $Al_{0.1}Ga_{0.9}N$ heterojunction provides 10 kT barrier to hole injection into the emitter.

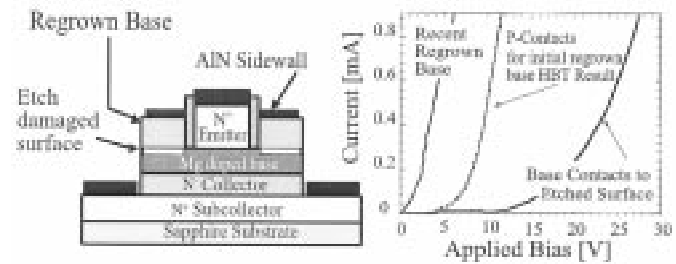

Fig. 2. Comparison showing the improvement resulting from a combination of a less-damaging etch and a regrown extrinsic base.

The difference between the base voltage under the base contact and the base voltage under the emitter mesa at any given base injection current is the parasitic offset voltage of the transistor. For example, it may require a 6 V base emitter contact voltage to inject a 100 μA base current. While the base-emitter junction forward bias is limited by the bandgap to 3.4 V, the base voltage under the base contact is ≈6 V. If the collector-emitter voltage is 3.4 V, the base-collector diode under the base contact is then forward biased even while the base-collector junction under the emitter mesa is zero-biased (Fig. 3). Also, because the contact characteristic is nonlinear, the voltage drop across the contact varies strongly with current density. This leads to a much larger voltage drop across the portion of the contact contributing to the lateral current which feeds the active transistor. This is indicated in Fig. 3 as a "battery" element. The following are equations for the collector current components in an HBT relevant to the common emitter offset voltage:

$$\mathbf{V}_{offset} \equiv \mathbf{V}_{CE}|_{I_C=0} \tag{1}$$

$$I_{C_{total}} = I_{CE} - I_{BC_i} - I_{BC_x} \tag{2}$$

$$I_{CE} = \alpha \cdot A_{emitter} \cdot J_{s\ BE} \cdot \exp\left[\frac{V_{BE}}{V_T}\right]. \tag{3}$$

If $V_{CB_{intrinsic}} \neq V_{CB_{extrinsic}}$

$$I_{BC_i} = A_{intrinsic} \cdot J_{s\ BC} \cdot \exp\left[\frac{V_{BC_i}}{V_T}\right] \tag{4}$$

$$I_{BC_x} = A_{extrinsic} \cdot J_{s\ BC} \cdot \exp\left[\frac{V_{BC_x}}{V_T}\right]. \tag{5}$$

Here we use α as an overall efficiency term that includes emitter injection efficiency as well as the transport efficiency across the base. Equations (4) and (5) split from a single equation when the external base-collector bias differs from the internal bias. In this case, a higher voltage is required to turn off the extrinsic base collector diode. Fig. 3 shows the contributions of the offset voltage equations to the total collector current, I_C. Analysis of a measured common emitter characteristic (Fig. 4) show these effects on the dc performance. To reduce this offset voltage, the base contact and lateral resistances must be reduced—or the extrinsic collector eliminated as in the transferred substrate Schottky collector technology [10].

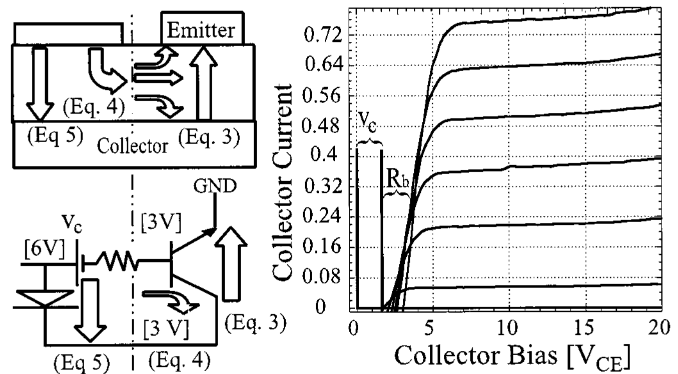

Fig. 3. Large parasitic offset is due to the voltage drop associated with lateral base current. The numbered arrows in the schematic (above left) refer to equations which describe them. The voltages in the wiring diagram (below left) are examples of a bias condition in which the parasitic base-collector diode is forward biased, while the intrinsic device is zero-based. This is the mechanism for the parasitic offset voltage observed in GaN HBTs.

IV. Regrown Emitter HBT

The motivation for the regrown emitter HBT is the lack of a need for an etch stop for the emitter mesa etch, and improved base contacts leading to lower parasitic base resistance and common emitter offset voltage. In addition, the regrown emitter HBT allows for more accurate base emitter junction placement than conventional structures grown by MOCVD because it is not subject to the Mg memory effect. The common emitter characteristics of a regrown emitter device in Fig. 5 show a current gain of 6, a low offset voltage, and an early voltage, $V_A > 400$ V. This preliminary result does not use a heterojunction emitter, suggesting that the current gain will be further improved in a regrown emitter HBT. The structure was grown by MOCVD on sapphire. The base thickness is 200 nm with an accepter concentration, $N_A = 5 \times 10^{19}$, leading to a carrier concentration of $p = 8 \times 10^{17}$ cm^{-3}. The emitter is GaN : Si, $N_D = 5 \times 10^{18}$ cm^{-3} 100 nm thick. The collector is 500 nm UID GaN with a background donor concentration of $N_D = 5 \times 10^{16}$ cm^{-3}. The initial device growth consisted of the subcollector, collector, and base layers. An AlN_x dielectric mask is patterned with openings for the emitter structure (Fig. 5). The emitter mesa is then grown selectively. The growth mask is removed, and device processing completed with the conventional Cl_2 RIE step to access the subcollector. Although attempts were made to selectively grow the emitter by MBE, these efforts have not yielded a working device. photo-electro-chemical (PEC) and wet etch techniques show promise for selectively etching n-type over p-type material [15], this etch would allow conventional processing of fully grown devices without the damage associated with the RIE etch. The etch stop becomes less effective, however, when the etch stop layer thickness, W_b is less than L_n, the diffusion length of electrons in the base—a necessary condition for transistor operation.

Although the regrown emitter device requires a regrowth interface in the base of the transistor, possibly leading to reduced transport or injection efficiency, it has achieved comparable current gain to etched emitter devices without the difficulties associated with the nonselective RIE emitter mesa etch and the base surface damage it causes. Circumventing these two major processing hurdles without degradation in performance makes the regrown emitter HBT a strong alternative to the conventional etched-emitter device.

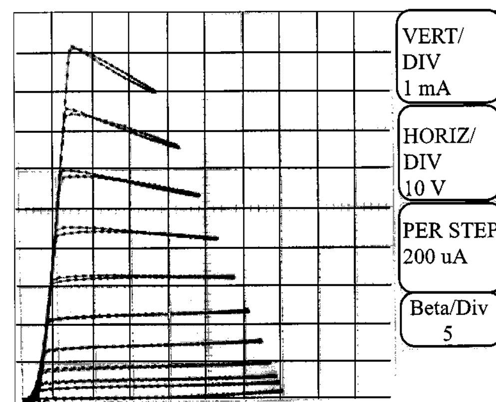

Fig. 4. Common emitter characteristics of regrown emitter BJT. The base current is stepped at 200 uA per step. The vertical axis is 1 mA/div. The current gain for this device, $\beta > 5$. The negative output resistance behavior of the collector is due to internal heating of the device.

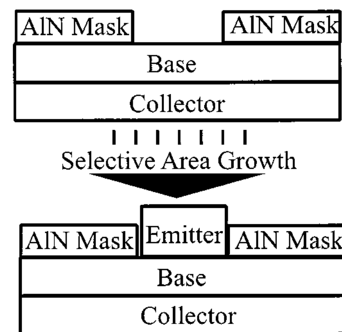

Fig. 5. Selective emitter regrowth step is shown above. The AIN_x mask is used to protect the base surface. The emitter structure is then selectively grown by MOCVD to form emitter mesas. Later, the mask is removed, and the base mesa is etched by Cl_2 RIE. Finally, base, emitter, and collector metallizations are applied using standard lift-off lithographic techniques.

V. HBT on LEO GaN

Both the regrown emitter and etched emitter structures suffer from of emitter collector leakage associated with threading dislocations (TDs). Due to the lattice mismatch between GaN and

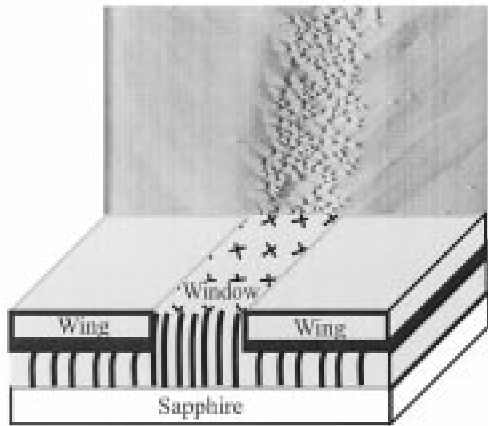

Fig. 6. Atomic force microscopy image of an LEO substrate (above) showing window and ring regions. Spiral growth mode in the window region is associated with the screw component of TDs. Wing regions consist of atomically flat steps.

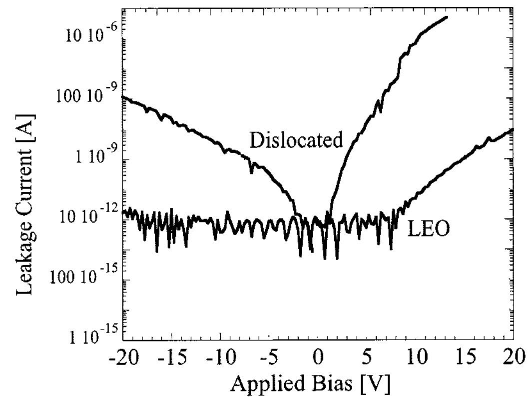

Fig. 7. Semi log plot of leakage current of LEO window compared to wing region. Plot shows reduction of leakage by four orders of magnitude for wing region as compared to window region. The emitter mesa area for these devices was $6\ \mu\text{m} \times 50\ \mu\text{m}$.

sapphire or SiC, thin GaN films ($\approx 2\ \mu$m) grown on these substrates have a TD density on the order of 5×10^8 cm^{-2}. To investigate the connection between TDs, doping, and collector-emitter leakage currents, devices were fabricated on material grown using the lateral epitaxial overgrowth technique, LEO. The details of the LEO process are described by Fini *et al.* [16]. LEO is well suited for this experiment because adjacent devices can be measured with and without dislocations. The window regions were 5 μm wide, repeated with a period of 40 μm. A full HBT structure is then grown on this sample by MBE. Over dislocated (window) regions the TDs continue, while over the wing regions, the lateral GaN growth is dislocation free. Fig. 6 shows the spiral MBE growth indicative of TDs with screw character [17] in the window region, and the lack of this spiral growth mode on the wing regions. The devices tested had emitter mesa areas of $6\ \mu\text{m} \times 50\ \mu\text{m}$. The collector-emitter leakage of adjacent devices was tested (Fig. 7) and was seen to drop by four orders of magnitude in the forward direction on the wing relative to the window. Common-emitter characteristics of an HBT on a wing region are shown in Fig. 8. The gain of the wing device is comparable to devices in the window (dislocated) regions. This result suggests that although dislocations are the dominating cause of collector-emitter leakage in these devices, at the present levels (10^8 cm^{-2}) they are not the cause of the high recombination rates in the base—which are expected to be related to the high Mg concentration (10^{20} cm^{-3}) and high levels of point defects. To our knowledge, this is the first demonstration of a GaN HBT on an LEO substrate. It conclusively demonstrates the connection between TDs and collector-emitter leakage.

VI. Collector-Emitter Leakage Explained

A reccurring problem with GaN HBTs has been the presence of significant collector-emitter leakage [5]. The GaN HBT on LEO (above) showed the connection between dislocations and leakage. The mechanism for collector-emitter leakage is found to be a localized punch-through effect. An experiment was performed in which two devices were fabricated, both with lightly doped bases ($N_A = 10^{19} \Rightarrow p = 10^{17}$ cm^{-3}) 100 nm thick, on areas of the same template with the approximately the same

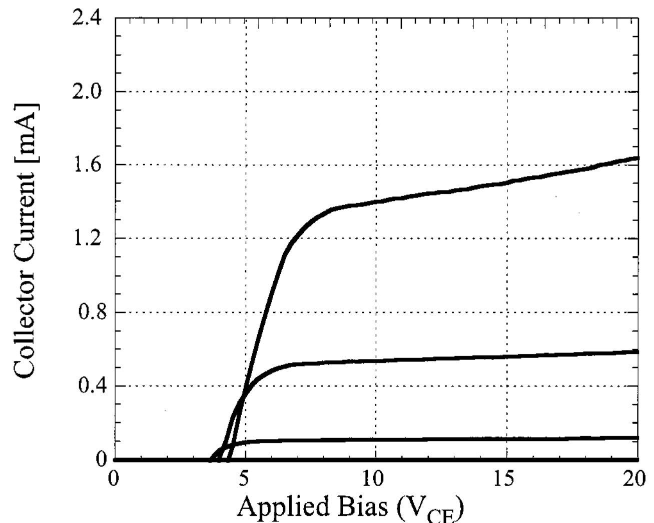

Fig. 8. Common emitter characteristics of GaN HBT on LEO wing (nondislocated region). Base current steps are $400\ \mu$A.

TD density (5×10^8 cm^{-2}). One of the samples was grown with a 15 nm p$^+$ ($N_A = 10^{20} \Rightarrow p = 10^{18}$ cm^{-3}) spike in the center of the base to block emitter/collector leakage. The results of this experiment (Fig. 9) show that the heavily doped spike in the neutral region of the base eliminated the emitter-collector short, suggesting that the mechanism for emitter-collector leakage is the local compensation of the base layer. The literature predicts that in n-type material TDs behave as electron traps, negatively charged when filled. In p-type material, the TDs are expected to behave as donors, or hole traps, and thus be positively charged [18]. Various energy levels have been predicted for midgap states associated with TDs ranging from 0.6 eV to 3.2 eV above the valence band [19]. Because the leakage was found to be dependent on both dislocation density and base doping, a hypothesis was developed for the mechanism of this leakage using the following model: We assume that each TD contributes a line of charge in p-type GaN equivalent to one donor for every 10 Å vertically, or 10^7 cm^{-1}. We simulate this as a column doped n-type at 3×10^{20} cm^{-3} and having a radius of 1 nm. The donor level is taken to be 3 eV above the valence

band edge. This level is chosen because it is consistent with a low-voltage punch through observed at lower doping levels, as well as the energetically favorable dislocation configuration in both Ga rich and N rich growth conditions [19]. Fig. 10 shows the effect of the local compensation on the p-type base. The result of this compensation in extreme cases—$N_A = 10^{19}$ cm^{-3} is a device that is shorted from collector to emitter. When the base doping concentration is sufficiently high—$N_A = 10^{20}$ cm^{-3}, however, a barrier remains to prevent the short. Although in this case the dislocations were found to be the dominant source of emitter-collector leakage, it should be noted that surface states and mesa sidewall damage may lead to emitter-base and base-collector leakage currents in addition to the dislocation induced leakage paths.

VII. Collector-Emitter Leakage and DC Characteristics

Because the collector-emitter leakage mechanism is a localized punch-through effect, it is isolated from the base contact. This isolation results in the misleading situation in which both the base-emitter and base-collector diodes appear to be rectifying when tested individually, while in fact the active device is shorted. This short is not seen in the base emitter diode because an intact lateral p–n junction blocks the current from the p-base to the local punch-through region. It is not seen in the base-collector diode due to the Schottky barrier from the base contact to the compensated region. As described in Section III the high base contact resistance and lateral base resistance cause a disparity between the base voltage under the contact and under the emitter mesa. When combined with a collector-emitter leakage mechanism, this voltage disparity causes Gummel plots to be unreliable for the determination of current gain. For example, if the base-emitter *contact* voltage is 10 V, and V_{CB} is set at zero, the actual collector-base voltage under the emitter mesa is 7 V reverse, and the collector-emitter voltage is 10 V. In devices that suffer from collector-emitter leakage, the forward current resulting from leakage may be greater than the current associated with the transistor action of the device. In this situation, the transistor current cannot be distinguished from the leakage current. A Gummel plot of a device with leakage current is shown in Fig. 11. Although the Gummel plot suggests a current gain of 50, the common emitter characteristic for the same device, Fig. 12, shows that the actual current gain is less than unity. Common base characteristics may also be misleading. This is because a collector-emitter leakage path will pass current without loss to the collector, and this may be misinterpreted as unity injection efficiency and transport. If the measurement is intended to demonstrate the transconductance of the device, care must be taken to drive the device with a voltage source rather than a current source. Transconductance is defined as $G_m = \partial I_C / \partial V_{BE}$. The parallel leakage path in the common base mode of the transistor may not be apparent when driven by a low output conductance current source, as the lower conductance of the source dominates. We conclude, therefore that when common-emitter characteristics are not useful due to emitter-collector leakage, common base and Gummel characteristics are not reliable in determining current gain.

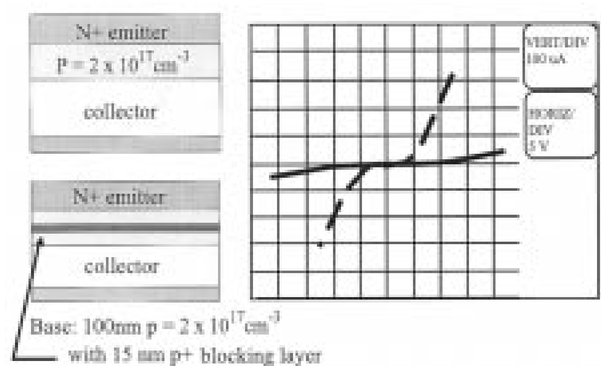

Fig. 9. Emitter-collector leakage is reduced by the addition of a p$^+$ spike in the neutral base of a transistor structure. The solid line represents the emitter-collector leakage of the device with the p$^+$ blocking layer, while the dashed line is corresponds to the device with a convectional base doped $p = 2 \times 10^17$ cm^{-3}.

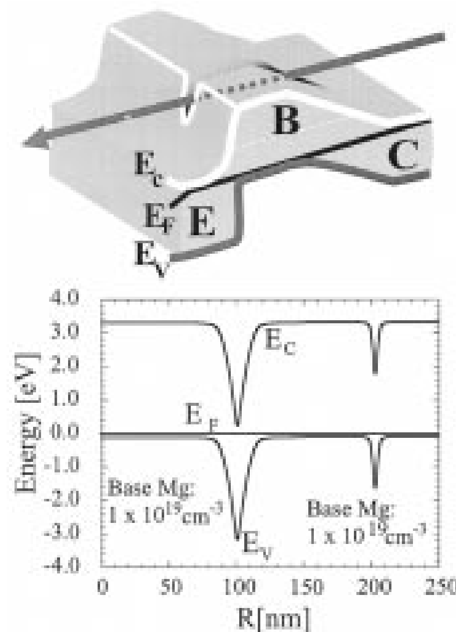

Fig. 10. Above: Three dimensional rendering of the band diagram of an HBT with a dislocation (arrow) causing local compensation of the p-type base. Below: Simulation of the band-diagram of a locally compensated area surrounding a dislocation in p-type GaN. A lightly doped base (left) is fully compensated near the dislocation, while a heavily doped base (right) is only partially compensated.

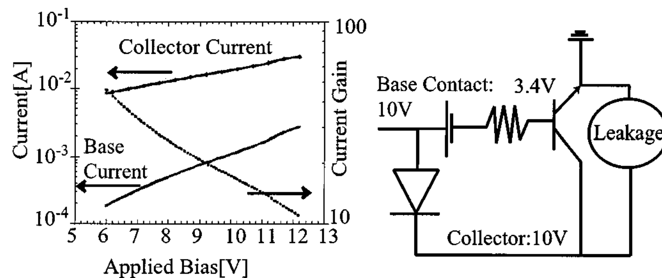

Fig. 11. Gummel plot of a bipolar transistor with emitter collector leakage. The current gain seems high, as the collector current is much greater than the base current. From the circuit diagram, however, we see an example bias condition where the collector-emitter voltage is large, even when $V_{BC} = 0$. Fig. 12 shows the common emitter characteristics for this device.

VIII. MAGNESIUM MEMORY EFFECT

The accepter dopant most commonly used for p-type GaN is magnesium. The Mg memory effect is common to many GaN MOCVD reactors. Etched-emitter devices are grown by MBE to avoid this problem. It is believed that due to the high Mg concentrations needed to adequately dope the p-type material, a substantial amount of Mg is left in an MOCVD reactor even after the flow is stopped. This Mg then incorporates into the film during subsequent growth. SIMS measurements of Mg levels in an NPN structure are shown in Fig. 13. The plot shows a large Mg tail past the point where the Si is turned on and the Mg turned off. Because HBTs are especially sensitive to emitter-base junction placement [20], a growth technique which can accurately define these junctions is required. MBE growth eliminate these effects and enables the achievement of Mg doping profiles that are orders of magnitude sharper than in MOCVD grown GaN : Mg films. Another advantage of N_2 source MBE over MOCVD when growing Mg-doped GaN is that no post-growth anneal is required to electrically activate the Mg atoms. The absence of hydrogen in the plasma-assisted MBE process makes this unnecessary. Also, the structures grown by MBE typically have lower background impurity concentration which has resulted in extremely high electron mobilities at low temperature in AlGaN/GaN HEMT structures [21]. Finally, we have found the MBE growth to be more reproducible with greater uniformity across the sample.

IX. CURRENT GAIN

The current gain of the GaN bipolar transistor is a major obstacle to the investigation of rf devices. The lifetime and the diffusivity of electrons in Mg doped GaN are unknown, but they are both expected to be low compared to practical base widths. This low lifetime is expected because of the high concentration of Mg in the base (between 5 and 10 $\times 10^{19}$ cm^{-3}) and high levels of point defects in Mg doped GaN [11]. Likewise, the electron velocity is expected to be adversely affected by the high base doping. Self consistent two-dimensional (2-D) numerical simulations indicate the expected current gain as a function of base width (Fig. 14). Although many key material properties in GaN are unknown, estimates can be used to gain useful insight into expected trends. For these simulations the electron lifetime used for the base was 25 ps. Minority carrier mobilities of $\mu_n = 100$ cm^2/Vs, $\mu_p = 10$ cm^2/Vs and the effective masses, $m_e = 0.19$ m$_0$, $m_h = 0.6$ m$_0$ were used. An advantage of AlGaN/GaN material system for HBT's is the large increase in bandgap with a relatively small Al composition:

$$E_g(\text{AlN}) - E_g(\text{GaN}) \approx 100 \cdot \text{kT}. \tag{6}$$

Suggesting that a compositional grade across the base of only 5% can result in an energy drop of 5 kT. Assuming the accepter level remains fixed relative to the valence band, this results in a quasifield in the base of

$$\vec{E}_q = \frac{5 \cdot \text{kT}}{qW_b}. \tag{7}$$

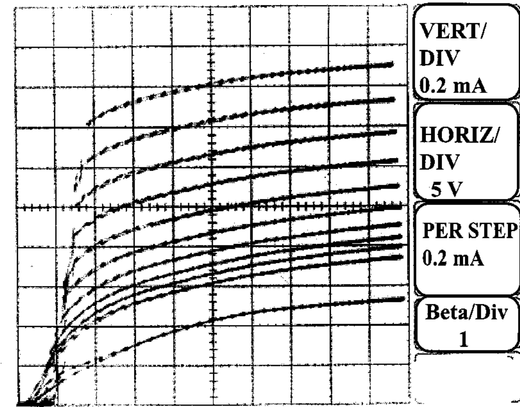

Fig. 12. Common emitter characteristics corresponding to Gummel plot in Fig. 11 Current gain is actually much lower than predicted by the Gummel plot.

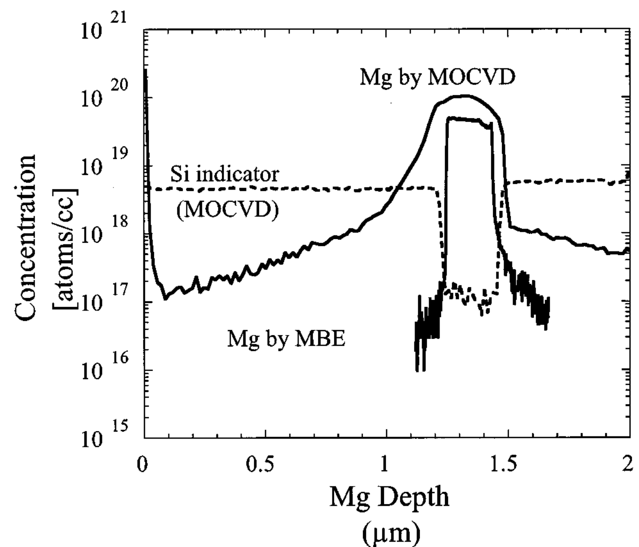

Fig. 13. SIMS study of Mg tail in emitter of an MOCVD grown n-p-n structure compared with MBE grown junctions. In the MOCVD case, the second junction has been displaced by 170 nm past the point where the flow was stopped (coincident with the Si turn-on). For MBE the Mg turn-off is much more abrupt (2.5 nm/dec).

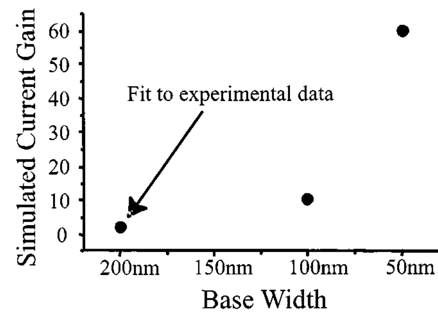

Fig. 14. Common emitter characteristics of an HBT with 5% Al grading in the base. The current gain of this device is approximately 1.5, three times that of a similar device without the grade. Base current steps are 500 μA/div. The collector current scale is 500 μA/div.

For a 100 nm base, the quasifield is then greater than 1.25×10^4 V cm^{-1}. Simulations reflecting this dependence of current gain with base compositional grading predict a dramatic

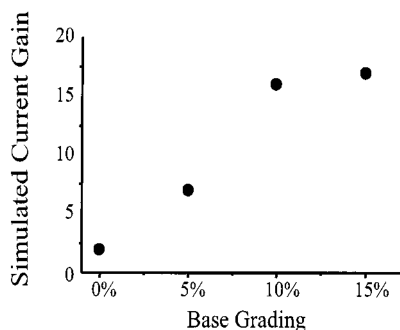

Fig. 15. Simulation of current gain enhancement as a function of base grading. Initial data point is experimental current gain value, and is used as a basis for the extrapolation for the data points with base compositional grading. The current gain is assumed to be limited by the minority carrier lifetime in the base, and is assumed not to be a function of Al composition.

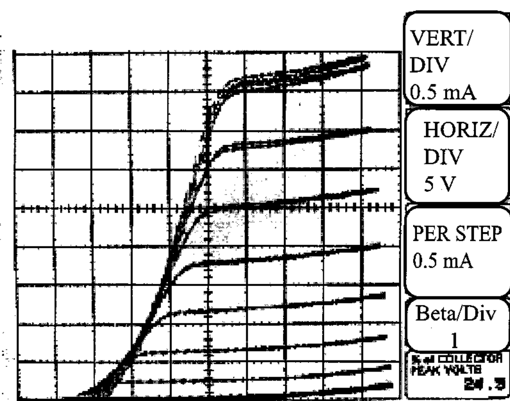

Fig. 16. Two-dimensional numerical simulation of current gain extrapolated from experimental data point as a function of base width. Simulation assumes that minority carrier lifetime in the neutral base is the limiting factor for current gain.

increase in gain for modest grading (Fig. 15). We have fabricated graded base devices and found some enhancement with Al compositional grading in the base (see Fig. 16).

X. Conclusions and Future Work

Calculations based on material properties show the great potential of the GaN HBT. Technological barriers to the realization of this potential include low base conductivity, the deep accepter-Mg, emitter collector leakage currents, and short electron lifetimes in the base. Selective area regrowth of base contact areas has demonstrated improvement of the extrinsic base conductivity, while emitter mesa regrowth was used to avoid etch damage, which is known to degrade base contacts. The use of LEO templates for HBTs has demonstrated the need for low dislocation densities in GaN for HBTs, and doping studies have confirmed the compensating nature of these dislocations in p-type GaN. Aluminum compositional grading in the base of an AlGaN/GaN HBT is expected to enhance carrier transport across the base, and common-emitter characteristics of a graded base device were presented. Although various hurdles remain in development of the rf GaN HBT, many of the initial barriers have been overcome. Future efforts will be concentrated on improving current gain, reducing base contact and bulk resistance, and developing processing techniques for rf compatible device structures and layouts. The recovery of etch-damaged surfaces will be investigated, and co-planar wave-guide structures fabricated for rf testing.

References

[1] Y. F. Wu *et al.*, "GaN-based FET's for microwave power amplification," *IEICE Trans. Electron.*, vol. E82-C, pp. 1895–1905, 1999.

[2] L. S. McCarthy *et al.*, "AlGaN/GaN heterojunction bipolar transistor," *IEEE Electron Device Lett.*, vol. 20, pp. 277–279, June 1999.

[3] J. B. Limb *et al.*, "High voltage operation ($>$80 V) of GaN bipolar junction transistors with low leakage," *Appl. Phys. Lett.*, vol. 76, pp. 2457–2459, 2000.

[4] S. Yoshida and J. Suzuki, "Characterization of a GaN bipolar junction transistor after operation at 300 degrees C for over 300 h," *Jpn. J. Appl. Phys.*, vol. 38, pp. L851–L853, 1999.

[5] B. S. Shelton *et al.*, "AlGaN/GaN heterojunction bipolar transistors grown by metal organic chemical vapor deposition," *Electron. Lett.*, vol. 36, pp. 80–81, 2000.

[6] S. Nakamura, "Development of violet InGaN-based laser diodes," *Oyo Buturi*, vol. 68, pp. 793–796, 1999.

[7] G. Parish, "High-performance (Al,Ga)N-based solar-blind ultraviolet p-i-n detectors on laterally epitaxially overgrown GaN," *Appl. Phys. Lett.*, vol. 75, pp. 247–249, 1999.

[8] U. V. Bhapkar and M. S. Shur, "Monte Carlo calculation of velocity-field characteristics of wurtzite GaN," *J. Appl. Phys.*, vol. 82, pp. 1649–1655, 1997.

[9] J. Kolnik, I. H. Oguzman, K. F. Brennan, W. Rongping, and P. P. Ruden, "Monte Carlo calculation of electron initiated impact ionization in bulk zinc-blende and wurtzite GaN," *J. Appl. Phys.*, vol. 81, pp. 726–733, 1997.

[10] Q. Lee, "Submicron transferred-substrate heterojunction bipolar transistors with greater than 8000 GHz f/sub max," in *Proc. IPRM*, 1999, pp. 175–178.

[11] P. Kozodoy, "Heavy doping effects in Mg-doped GaN," *J. Appl. Phys.*, vol. 87, pp. 1832–1835, 2000.

[12] H. Katayama-Yoshida, T. Nishimatsu, T. Yamamoto, and N. Orita, "Codoping in wide band-gap semiconductors," in *Proc. ISCS*, 1998, pp. 747–756.

[13] J. S. Im, "Radiative carrier lifetime, momentum matrix element, and hole effective mass in GaN," *Appl. Phys. Lett.*, vol. 70, pp. 631–633, 1997.

[14] J. Ja-Soon, P. Seong-Ju, and S. Tae-Yeon, "Formation of low resistance Pt ohmic contacts to p-type GaN using two-step surface treatment," *J. Vac. Sci. Technol. B*, vol. 17, pp. 2667–2670, 1999.

[15] A. R. Stonas *et al.*, "Backside-illuminated photoelectrochemical etching for the fabrication of deeply undercut GaN structures," *Appl. Phys. Lett.*, vol. 77, pp. 2610–2612, 2000.

[16] P. Fini *et al.*, "High-quality coalescence of laterally overgrown GaN stripes on GaN/sapphire seed layers," *Appl. Phys. Lett.*, vol. 75, pp. 1706–1708, 1999.

[17] B. Heying, "Dislocation mediated surface morphology of GaN," *J. Appl. Phys.*, vol. 85, pp. 6470–6476, 1999.

[18] K. Leung, A. F. Wright, and E. B. Stechel, "Charge accumulation at a threading edge dislocation in gallium nitride," *Appl. Phys. Lett.*, vol. 74, pp. 2495–2497, 1999.

[19] L. S. Mi *et al.*, "Electronic structures of GaN edge dislocations," *Phys. Rev. B, Condens. Matter*, vol. 61, pp. 16 033–16 039, 2000.

[20] S. M. Sze, *Physics of Semiconductor Devices*, 2nd ed. New York: Wiley, 1981.

[21] C. R. Elsass *et al.*, "High mobility two-dimensional electron gas in AlGaN/GaN heterostructures grown by plasma-assisted molecular beam epitaxy," *Appl. Phys. Lett.*, vol. 74, pp. 3528–3530, 1999.

Lee S. McCarthy received the B.S. (1996) and M.S. degrees in electrical engineering from the University of California, Santa Barbara (UCSB).

He has been working under U. K. Mishra with the bipolar electronics team at UCSB, which demonstrated the first GaAs/GaN fused heterojunction diode in 1997, the first AlGaN/GaN bipolar transistor in 1998, the first GaN HBT on LEO GaN in 2000 and the first rf measurements of an AlGaN/GaN HBT in September, 2000. He was previously with Nitres Inc., Goleta CA, where he fabricated the first GaN pnp bipolar transistor in 1999. He is currently a Principal Engineer for Device Fabrication at Nitronex Corporation, Raleigh, NC, working on the development of AlGaN/GaN electronics.

Ioulia P. Smorchkova received the M.S. degree in applied physics from V. I. Uly'anov (Lenin) Leningrad Electrical Engineering Institute, Russia, in 1992, and the Ph.D. degree in physics from Pennsylvania State University, University Park, in 1998.

She is currently employed at the University of California, Santa Barbara, as a Research Engineer. Her research focuses on molecular beam epitaxy of GaN-based semiconductor structures for electronic device applications. She has authored and co-authored over 30 publications.

Huili Xing received the B.S. degree in physics at Peking University, China, in 1996, and M.S. degree in material science and engineering from Lehigh University, Bethlehem, PA, in 1998. She is now working under the direction of U. K. Mishra on GaN bipolar electronics at the University of California, Santa Barbara.

P. Kozodoy, photograph and biography not available at the time of publication.

Paul Fini received the Ph.D. degree in materials science (emphasis electronic materials) in Oct. 2000 from the University of California, Santa Barbara (UCSB).

He is currently with UCSB as a Staff Scientist and Lead Researcher of S. Nakamura's research group. His research interests include thin-film and bulk growth of GaN and related materials, lateral epitaxial overgrowth, and structural and morphological characterization. He has authored or co-authored over 47 publications and 38 conference presentations.

J. Limb, photograph and biography not available at the time of publication.

David L. Pulfrey (F'00) received the B.Sc. and Ph.D. degrees in electrical engineering from the University of Manchester, U.K., in 1965 and 1968, respectively.

Since 1968, he has been on the faculty of the Electrical Engineering Department, University of British Columbia (UBC), Vancouver, BC, Canada. His research area is semiconductor device modeling. He is the author of *Photovoltaic Power Generation* (Van Nostrand Reinhold, 1979), and, with G. Tarr, *Introduction to Microelectronic Devices* (Prentice-Hall, 1989). He has published over 105 articles on the topics of: compact modeling of HBTs, quantum-well lasers, solar cells and UV photodiodes; electrical breakdown in thin dielectrics; the preparation and properties of plasma-anodized thin oxide films; the analysis and fabrication of surface junction solar cells; the modeling and reliability of high-gain polysilicon-emitter transistors; the analysis of silicon MIS tunnel junction structures and related devices; and circuit techniques and algorithmic macrocell generation for CMOS VLSI.

Dr. Pulfrey was elected Fellow of IEEE in 2000 for contributions to the modeling of heterojunction bipolar semiconductor devices. He was the inaugural winner of UBC's Teaching Prize for Engineering in 1990.

James S. Speck is a Professor in the Materials Department at the University of California, Santa Barbara. His work focuses on the relationship between growth, microstructure and physical properties in wide bandgap and "conventional" III–V semiconductors and in ferroelectric thin films.

Mark J. W. Rodwell (M'89–SM'99) received the B.S. degree from the University of Tennessee, Knoxville, in 1980, and the M.S.and Ph.D. degrees from Stanford University, Stanford, CA, in 1982, and 1988, respectively.

He is Professor and Director of the Compound Semiconductor Research Laboratories, University of California, Santa Barbara (UCSB). He was with AT&T Bell Laboratories from 1982 to 1984. His research focuses on very high bandwidth bipolar transistors, high speed bipolar IC design, and GHz mixed-signal ICs. His group has worked extensively in the area of GaAs Schottky-diode ICs for subpicosecond/mm-wave instrumentation.

Dr. Rodwell is the recipient of a 1989 National Science Foundation Presidential Young Investigator Award, and his work on submillimeter-wave diode ICs was awarded the 1997 IEEE Microwave Prize.

S. P. Denbaars, photograph and biography not available at the time of publication.

U. K. Mishra (S'80–M'83–SM'90–F'95) received the B.Tech. degree from the Indian Institute of Technology, Kanpur, India, the M.S. degree from Lehigh University, Bethlehem, PA, and the Ph.D. degree from Cornell University, Ithaca, NY, in 1979, 1980, and 1984, respectively, all in electrical engineering.

He has worked in various laboratory and academic institutions, including Hughes Research Laboratories, Malibu, CA, University of Michigan, Ann Arbor, and General Electric, Syracuse, NY, where he has made major contributions to the development of AlInAs–GaInAs HEMTs and HBTs. He is now a Professor in the Department of Electrical and Computer Engineering, University of California, Santa Barbara. His current research interests are in oxide based III–V electronics and III–V nitride electronics and opto-electronics. He has authored or co-authored over 400 papers in technical journals and conferences and holds six patents.

Dr. Mishra was a co-recipient of the Hyland Patent Award given by Hughes Aircraft, and the Young Scientist Award presented at the International Symposium on GaAs and Related Compounds.